Korean J. Chem. Eng., 39(4), 1036-1044 (2022)
DOI: 10.1007/s11814-021-0944-8

pISSN: 0256-1115
eISSN: 1975-7220

Effect of nano MMT and mesoporous MCM-41 on corrosion resistance of poly (propylene carbonate) - based waterborne polyurethane

Jiaying Zhang*,†, Hui Zheng*, Haibo Geng*, Ying Li*, Yapeng Guan*, Yuanbin Sun, and Cunjian Zhu****

*Department of Food and Drug Engineering, Shijiazhuang University of Applied Technology, No 12 Changxing Street, Qiaoxi District, Shijiazhuang Hebei 050081, China
**Shijiazhuang Flagship Coating Technology Co., Ltd., No 120 Huanghe Avenue, Gaoxin District, Shijiazhuang 050000, Hebei, China
(*Received 25 April 2021 • Revised 28 August 2021 • Accepted 30 August 2021*)

Abstract−Environmental friendly poly (propylene carbonate)-based waterborne polyurethane (PPC-based WPU) is prepared with PPC and isophorone diisocyanate (IPDI) as the soft segment and the hard segment, respectively. In this reaction system, 2,2-dimethylolbutyric acid (DMBA) is used as the hydrophilic donor and trimethylolpropane (TMP) as the crosslinking agent. The effect of co-doping of layered montmorillonite (MMT) and mesoporous material MCM-41 on corrosion resistance of PPC-based WPU resin was studied. The properties of the samples were characterized with N_2 physical adsorption, XRD, FT-IR, TG-DTA, DSC and water absorption testing. Potentiodynamic polarization curves, electrochemical impedance spectroscopy (EIS) and salt spray test were employed to investigate the corrosion performance of all the coatings. The results of XRD indicate that the MMT in the composite polyurethane resin is peeled off and MCM-41 maintains the hexagonal framework structure after grinding. Compared with the WPU coatings with MMT or MCM-41 single incorporation, those with MMT and MCM-41 co-incorporation show the best corrosion resistance, which is due to the different interface structure between filler and resin matrix.

Keywords: Corrosion Resistance, Nanocomposites, Propylene Carbonate Polyols, Waterborne Polyurethane

INTRODUCTION

Steel corrosion is a common problem in large buildings and steel construction industrial equipment. Corrosion reduces the thickness of steel and reduces the supporting force. In serious cases, it leads to equipment aging and failure, and at the same time, polluting production materials and even causing accidents.Therefore, how to prevent the corrosion of steel construction has great economic and social value. At present, the most direct anti-corrosion protection methods include shielding, passivation and electrochemical protection [1-3]. Solvent based coatings still play a leading role in steel structure anti-corrosion.

In recent years, with the gradual enhancement of awareness of environmental protection and the increasingly stringent environmental protection legislation of governments in various countries, the development of pollution-free, high-performance and economical anticorrosive coatings has become a development trend. More and more metal anti-corrosion coatings are changing to the direction of environmentally friendly waterborne [4,5]. Resins commonly used in waterborne anticorrosive coatings include waterborne acrylic resin, waterborne polyurethane resin, waterborne alkyd resin and waterborne epoxy resin [6-11]. Due to the environmental protection and free regulation performance, waterborne polyurethane has been gradually used in waterborne anticorrosive coatings. For waterborne polyurethane, the type of soft segment has a key impact on the resin properties and the final coating performance. Poly (propylene carbonate) polyol (PPC) is a new type of aliphatic polycarbonate polyol, which is prepared by copolymerization of propylene oxide and carbon dioxide [12]. The synthesis of PPC is characterized by abundant raw materials, cheap catalyst and simple operation. It is of great significance to reduce production cost and comprehensive utilization of carbon dioxide. The content of carbon dioxide in the synthesized PPC molecule accounts for 31%-50%, which not only greatly reduces the consumption of upstream raw material petroleum, but also relieves the greenhouse effect caused by carbon dioxide emission. Due to the existence of polycarbonate structure in PPC molecular structure, the barrier properties of resin and corresponding coating prepared by this material are improved [13].

The addition of nano-particles could improve the performance of paints, for instance, mechanical behavior, corrosion resistance and UV resistance. The addition of proper fillers can effectively improve the barrier performance of organic coatings. There have been many reports on the use of nanoparticles, such as Ti, SiO_2, TiO_2, ZrO_2 and Zn, to improve the corrosion resistance of coatings [14-18]. The physicochemical properties of epoxy resin/montmorillonite (MMT) composites were dramatically improved by introducing nano MMT into epoxy resin [19]. The corrosive resistance of mild steel could be obviously improved by organic modified MMT reinforced epoxy resin [10].

The synthesis and characterization of polymerizate/MCM-41 complex materials has become a hot topic [20-22]. Mesoporous

†To whom correspondence should be addressed.
E-mail: shenao_07@163.com

MCM-41 has been employed as a reinforcing material to improve the physicochemical nature of polymeric materials owing to its large specific surface area, adjustable texture height, long-range ordering, controllable pore size. Significant reinforcement and toughening effects can also be obtained by co-doping of nano MMT and mesoporous MCM-41 into polypropylene [23].

However, the application of co-doping of nano MMT and mesoporous MCM-41 in waterborne polyurethane coatings has not been reported yet. The metal corrosion protection effect of poly (propylene carbonate)-based waterborne polyurethane (PPC-based WPU) is rarely reported. In this paper, the PPC-based WPU was synthesized with PPC as the soft segment and the effects of the addition of MMT and MCM-41 on the anti-corrosion performance of the PPC-based WPU coatings were investigated by potentiodynamic polarization curves, electrochemical impedance spectroscopy (EIS) and salt spray test.

EXPERIMENTAL

1. Materials

PPC (Mn=3,000 g mol^{-1}) was purchased from Guangdong Dazhi Environmental Technology Co., Ltd. (China). Isophorone diisocyanate (IPDI), triethylamine (TEA), acetone, 2,2′-Bis(hydroxymethyl) butyric acid (DMBA), 1,4-Butanediol (BDO), trimethylolpropane (TMP) and dibutyltin dilaurate (DBTDL) were provided by Tianjin Damao Chemical Reagent Factory (China). Montmorillonite (MMT), mesoporous MCM-41 and 4 Å molecular sieve were supplied by Shanghai Macklin Biochemical Co., Ltd. (China). The experimental water was provided by the deionized water supply center of Shijiazhuang University of Applied Technology. Before use, PPC and BDO were dehydrated at 120 °C for 4 h under vacuum and DMBA was dehydrated at 140 °C for 3 h. Acetone and TEA were dehydrated by 4 Å molecular sieve before use for 12 h.

2. Preparation of PPC-based WPU Emulsion

81.1 g PPC and 28.8 g IPDI were charged into a 500 ml, 4-neck flask equipped with N_2 protection and stirred for approximately 10 min at 300 rpm. When the temperature was heated to to 60 °C, a few drops of DBTDL were added to the mixture under continuous stirring. The reaction temperature continued to rise to 80 °C and was kept for 2 h. 7.8 g DMBA was added and the reaction was kept at 80 °C for 3 h. After cooling to 60 °C, 1.2 g TMP and 1.2 g BDO were added and then reacted for 2 h. The mixture was then cooled to 40 °C and stoichiometric TEA was added to the mixture as a neutralizer to react for 30 min (pH=6). In the process of reaction, proper amount of acetone can be added to adjust the viscosity. After the neutralization, stoichiometric deionized water was added into the mixture and stirred vigorously at approximately 700 rpm for 1 h. Then, acetone was removed from the reaction system by vacuum rotary evaporation, and PPC-based waterborne polyurethane was obtained.

3. Preparation of PPC-based WPU Nanocomposite Emulsion

First, the physically adsorbed water on the surfaces of MMT and MCM-41 was removed by treating in vacuum oven at 80 °C for 1 h and then added directly to the PPC based WPU with deionized water as solvent. The ratio between the PPC-based waterborne polyurethane and solvent was 4 : 1. A multifunctional dispersive grinding machine was employed as the mixing equipment. The mixture was ground for 40 min with a rotation rate of 3,000 rpm. The addition amount of MCM-41/MMT particles in the nanocomposite emulsion was 0 wt%/0 wt%, 1.0 wt%/0 wt%, 0 wt%/1.0 wt%, 0.25 wt%/0.25 wt%, 0.5 wt%/0.5 wt% and 0.75 wt%/0.75 wt%, respectively. According to the addition amount of MCM-41 and MMT particles in the emulsion, the samples were designated as WPU, MCM-41/WPU, MMT/WPU, MCM-41-MMT(0.25)/WPU, MCM-41-MMT(0.5)/WPU and MCM-41-MMT(0.75)/WPU, respectively.

4. Preparation of PPC-based WPU Emulsion Film and Coating

A certain amount of emulsion was poured onto the polytetrafluoroethylene (PTFE) plate and cast into film, naturally dried for four days at room temperature, then dried at 60 °C for three days in vacuum drying oven and kept in the dryer for standby.

The steel plate with rounded corners and edges (145 mm×70 mm×0.5 mm) was sanded with a fine emery paper, successively washed with acetone and anhydrous alcohol, dried and then used as backup. The liquid coatings of all samples with 50±3 μm were coated with a wound rod and cured in a constant temperature and humidity box at 25 °C for seven days. The thickness of cured coatings was measured with a high precision coating thickness gauge (TT260A).

5. Characterization

Nitrogen adsorption-desorption isotherms of samples were achieved with an ASAP 2020 (Micromeritics) apparatus at −196 °C and samples were degassed at 200 °C for 4 h before testing. The X-ray diffraction (XRD) (Rigaku, D-MAX-2500-PC) apparatus was employed to analyze the crystalline phases of samples with Cu Ka radiation (λ=1.54056 Å) operated at 50 kV and 100 mA. To determine the functional groups and chemical structure of PPC and PPC-based WPU, Fourier transform infrared (FT-IR) transmission spectra were obtained by Nicolet MNGNA-IR560 with 4 cm^{-1} resolution. Differential scanning calorimetry (DSC) curves were achieved by a DSC-Q10 (TA Instruments, America) differential scanning calorimeter in nitrogen atmosphere (50 ml min^{-1}) from −50 to 250 °C with a heating rate of 10 °C min^{-1}. The thermal analysis system of the instrument was adopted to analyze the data of DSC to obtain the glass transition temperature (T_g). The thermal properties of the samples were investigated by thermogravimetric and differential thermal analysis (TG-DTA) on a NETZSCHSTA 409 PC thermo analyzer within a temperature range from 30 to 800 °C with a heating rate of 10 °C min^{-1} in N_2 flow. A water absorption test was carried out at room temperature and the detailed operation steps were as follows: the PPC-based WPU films were cut into squares of 2 cm×2 cm, weighed (m_1), and then soaked in water for 24 h, wiping the surface of the films with filter paper and weighed (m_2). The water absorption was calculated according to the following equation:

$$\text{Water absorption} = \frac{m_2 - m_1}{m_1} \times 100\% \quad (1)$$

6. Corrosion Performance Tests

An electrochemical workstation with a three-electrode system (CHI660D, CH Instruments, USA) was employed to perform electrochemical measurements of the coatings. For the electrochemical workstation, the coated sample was used as the working electrode,

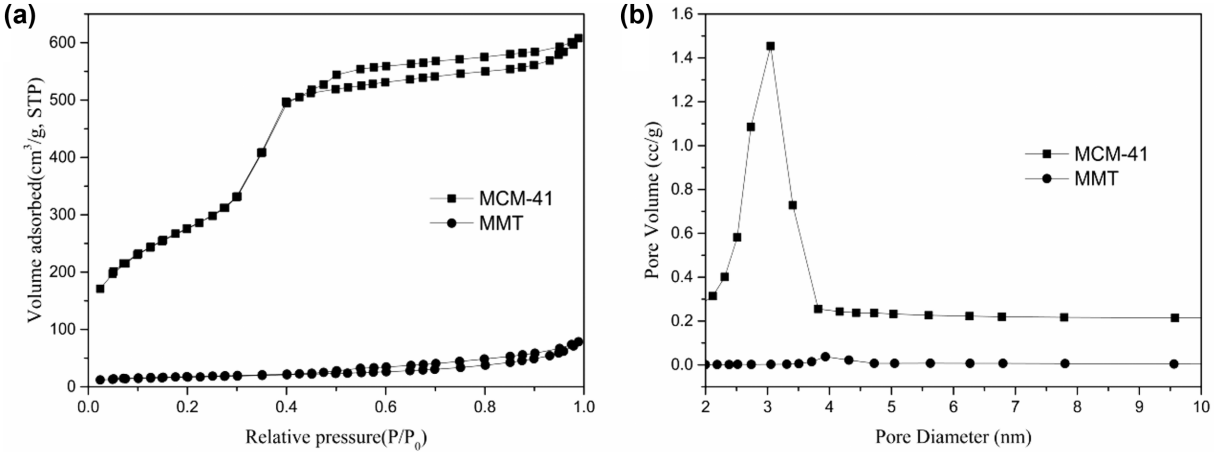

Fig. 1. (a) N_2 physical adsorption-desorption curves of MCM-41 and MMT and (b) The pore size distribution curves of MCM-41 and MMT.

an Ag/AgCl electrode and a stainless steel cylinder acted as the reference electrode and the counter electrode, respectively. The measurement area of the working electrode was ~14 cm^2 and the experimental data were normalized to 1 cm^2. All measurements were carried out in a 3.5 wt% sodium chloride aqueous solution at ambient temperature, and prior to the measurement the coated sample was soaked for 0.5 h to guarantee steady-state, and all tests were repeated at least three times. For the polarization current test, the corrosion current (I_{corr}) and the corrosion potential (E_{corr}) were automatically gained from the Tafel curve by the CHI660D workstation analysis software. For the electrochemical impedance spectroscopy (EIS) test, impedance spectra of the coated sample were recorded in the frequency range from 10^{-2} to 10^5 Hz with a sinusoidal AC perturbation of 10 mV. Finally, a salt spray test was performed on a salt spray test chamber (LX-60A, Guangdong Aisirui Instrument Technology Co., Ltd) to evaluate the corrosion performance of the coated sample. According to ASTM B117, the test conditions of the test chamber were set as continuous spraying with 5.0 wt% sodium chloride solution for 5 days at 35±2 °C. After the experiment, the surface of the coated sample was monitored by visual inspection, and the degree of rust was graded.

RESULTS AND DISCUSSION

1. Characterization of PPC-based WPU Nanocomposite

1-1. Physical Property

The physical properties of MCM-41 and MMT were characterized by N_2 adsorption-desorption isotherms and the results are shown in Fig. 1. Fig. 1(a) and (b) show the N_2 adsorption-desorption isotherms and the pore size distribution curves of MCM-41 and MMT, respectively. As shown in Fig. 1(a), the N_2 adsorption isotherm of MCM-41 increased sharply at P/P_0=0.3-0.4 , which is classified as typical type IV according to IUPAC [23] and that of MMT shows a typical type III, which means no mesoporous structure. The textural properties of MCM-41 and MMT are collected in Table 1.

1-2. XRD Analysis

Fig. 2 shows the low angle XRD patterns of MCM-41, MMT, MCM-41/WPU, MMT/WPU and MCM-41-MMT(0.5)/WPU. It can be seen in Fig. 2 curve (a) that the diffraction peaks of MCM-41 at 2.3, 3.9 and 4.5° correspond to the (100), (110) and (200) planes of typical mesoporous MCM-41, respectively, which indicates a good hexagonal long-range ordered arrangement [24]. In Fig. 2 curve (b), the pure MMT exhibits a diffraction peak at 5.7° corresponding to the (001) plane of typical layered MMT. It can be observed from the XRD pattern of MMT/WPU (Fig. 2 curve (d)) that the diffraction peak began to move to the small angle position and became wider, indicating that the MMT layers were intercalated. Curve (c) for MCM-41/WPU and curve (e) for MCM-41-MMT(0.5)/WPU are very similar and both present typical XRD

Table 1. The textural properties of MCM-41 and MMT

Samples	BET specific surface (m^2/g)	Total hole volume (cc/g)	Average aperture radius (nm)
MCM-41	1,304	1.02	3.06
MMT	59	0.12	3.94

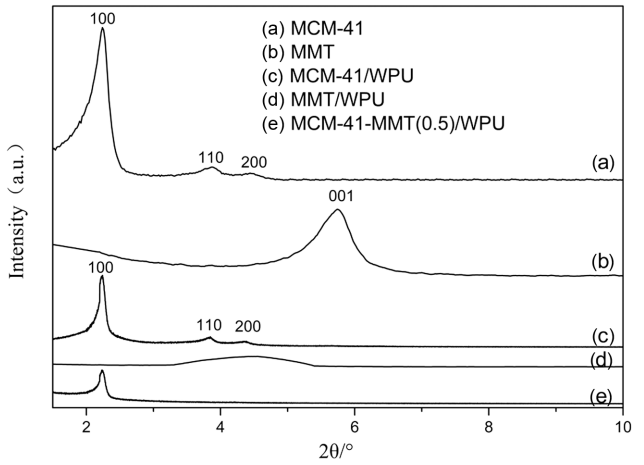

Fig. 2. Low angle XRD patterns of MCM-41, MMT, MCM-41/WPU, MMT/WPU and MCM-41-MMT(0.5)/WPU.

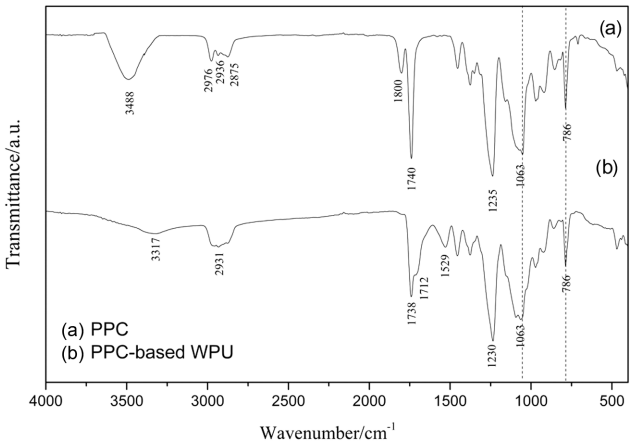

Fig. 3. FT-IR spectra of PPC and PPC-based WPU.

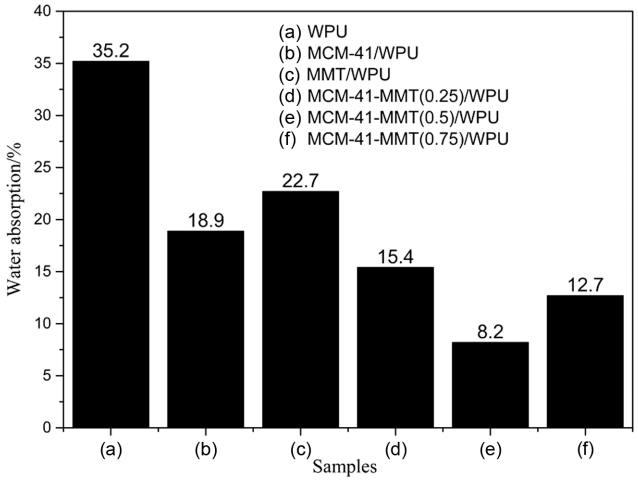

Fig. 4. Effect of MMT and MCM-41 on water absorption of samples.

patterns of MCM-41, which indicates that the hexagonal framework structure of of MCM-41 was preserved. In the curve e, the characteristic diffraction peak of MMT is not observed in curve (e), indicating that it disappeared or was covered by that of MCM-41. This may mean that the MMT layer was peeled off or intercalated to a certain extent,which was similar to that of Wang et al. [23,25].

1-3. FT-IR Spectroscopy

FT-IR spectra were employed to characterize the molecular structure of PPC and PPC-based WPU and the results are shown in Fig. 3. For PPC, as shown in Fig. 3 curve (a), the strong absorption peak at 3,488 cm^{-1} belongs to OH group, and the two relatively weak absorption peaks at 2,936 cm^{-1} and 2,875 cm^{-1} belong to the stretching vibration of -CH_3 and -CH_2, respectively. The C=O and C-O stretching vibrations of the O-C=O group led to two strong absorption peaks at 1,740 cm^{-1} and 1,263 cm^{-1}, respectively [26]. The characteristic absorption peaks of cyclic carbonate appeared at 1,800 cm^{-1} and 786 cm^{-1} and the absorption peak at 1,063 cm^{-1} was attributed to the stretching vibrations of O-C-O [27].

For PPC-based WPU, as shown in Fig. 3 curve (b), the strong absorption peak of OH group at 3,488 cm^{-1} disappeared, while new characteristic absorption peaks appeared at 3,317 cm^{-1} and 1,529 cm^{-1}, which could be attributed to the stretching vibration and bending vibration of N-H group, respectively. The C=O stretching vibration of the N-C=O group appeared at 1,712 cm^{-1} as the shoulder absorption peak. The absorption peak of carbamate bond (-NHCO-) appears at 1,529 cm^{-1}, which was formed by the reaction of -OH and -NCO. Meanwhile, the characteristic absorption peak at 1,800 cm^{-1} assigned to cyclic carbonate disappeared, indicating that the ring opening reaction of cyclic carbonate took place and participated in the formation of polyurethane molecules. The absorption peak of of NCO group at at 2,270 cm^{-1} disappeared, indicating that the NCO group had reacted completely. The characteristic peaks the C=O and C-O stretching vibrations of the O-C=O group of PPC-based WPU shifted to the lower frequency after the reaction of PPC, and appeared at 1,738 cm^{-1} and 1,230 cm^{-1}, respectively.

1-4. Water Adsorption Measurement

For waterborne anti-corrosive coatings, they are often in a working environment with high humidity. Water in the working environment often accelerates the corrosion reaction. Therefore, the water resistance of waterborne anti-corrosion coatings has a significant impact on their corrosion resistance. Waterborne anti-corrosive coatings with good water resistance often show excellent corrosion resistance. Generally, the water resistance of coatings is characterized by testing the water adsorption of the sample.

The effect of MMT and MCM-41 on the water resistance of samples was studied by testing the water absorption of each sample and the results are in Fig. 4. As shown, the water absorption rate of WPU was 35.2% after 24 h soaking, while those for MCM-41/WPU and MMT/WPU were 18.9% and 22.7%, respectively. The results show that the addition of MCM-41 and MMT was helpful to improve the water resistance of WPU, and the effect of MCM-41 was better than MMT with the same addition amount. As a comparison, the water absorption of MCM-41-MMT(0.5)/WPU was also tested. It was found that MCM-41-MMT(0.5)/WPU showed the lowest water absorption with the same total addition, indicating the best water resistance. This indicates that MMT and MCM-41 played a synergistic role in the formation of space network structure by increasing the cross-linking degree of the system. To determine the optimal amount of MMT and MCM-41, the water absorption of MCM-41-MMT(0.25)/WPU and MCM-41-MMT(0.75)/WPU was also tested. As shown in Fig. 4, with the increase of the amount of nanoparticles, the water absorption of the samples first decreased and then increased and MMT-MCM-41(0.5)/WPU showed the lowest water absorption with 8.2%. This shows that the excessive addition of nanoparticles will reduce the water resistance of the sample, and the optimal total addition amount was 1.0 wt% with 1 : 1 mass ratio of MCM-41 to MMT.

1-5. DSC Analysis

Exothermic peaks in DSC curves of PPC based WPU films indicated that chemical bonds may be formed at the interface with WPU substrate during the curing process. The DSC curves of the samples were analyzed by the system software, and the relevant data such as glass transition temperature (T_g), melting temperature (T_m) and the heat of reaction (ΔH) were obtained, as shown in Table 2.

Table 2. T_g, ΔH and T_m characteristics of the samples

Samples	T_g (°C)	ΔH (J/g)	T_m (°C)
WPU	−18.6	5.5	177.8
MCM-41/WPU	−12.3	9.1	178.5
MMT/WPU	−15.7	7.8	178.1
MCM-41-MMT(0.5)/WPU	−9.2	12.9	179.9

According to Table 2, there was only one T_g for PPC-based WPU coatings. It had been reported that PPC-based WPU was amorphous. Because a large number of carbonate and ether bonds exist in PPC molecules, it was easy to form intramolecular and intermolecular hydrogen bonds. Therefore, the phase separation of PPC-based WPU was not obvious, and there was only one T_g [28]. In all samples, MCM-41-MMT(0.5)/WPU showed the maximum exothermic heat. This may be due to the exfoliation of MMT and the formation of PPC-based WPU chain in the mesoporous channel of MCM-41, which improved the degree of cross-linking and it was consistent with the results of XRD. Shi et al. [16] reported that the cross-linking degree of the high solid epoxy resin was closely related to T_g that higher degree of cross-linking corresponded to higher T_g. For MCM-41-MMT(0.5)/WPU, the shift of T_g to higher temperature may be due to the strong interaction between nanoparticles and PPC-based WPU. In addition, owing to the cooperative effect, the combination of two nanomaterials with different shapes may more effectively promote the interaction [23]. With the increase of cross-linking degree, the compactness of the coating was better, which corresponded to the better impermeability.

1-6. TGA Analysis

The effects of MMT and MCM-41 on the thermal degradation behavior of PPC-based WPU films were studied by TGA technology and the results are shown in Figs. 5 and 6, and Table 3. There are two obvious thermal decomposition stages for typical polyurethane. The first stage is the decomposition of hard segment (carbamate) at 250-300 °C, and the second stage is the decomposition of soft segment (polyol) at 350-410 °C [29]. However, the decomposition temperature of pure PPC is 230-260 °C [30]. Therefore, the decomposition temperature of PPC is lower than that of carbamate.

Figs. 5 and 6 show TGA and DTG curves of different PPC-based WPU films. The 5% weight loss temperature ($T_{d,0.05}$), the 10% weight loss temperature ($T_{d,0.10}$), the 50% weight loss temperature ($T_{d,0.50}$) and the temperature at the maximum weight loss rate

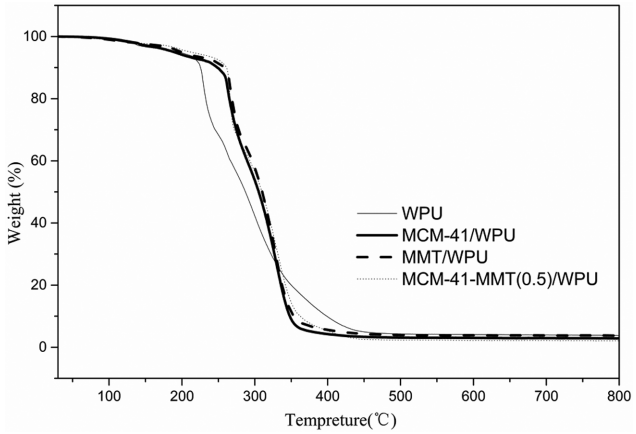

Fig. 5. TGA curves of PPC-based WPU films.

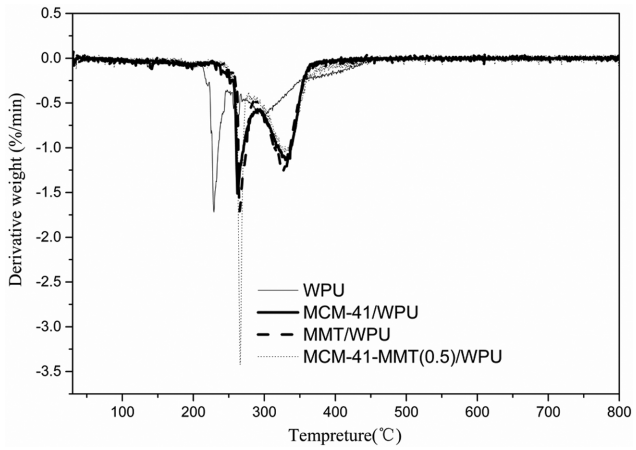

Fig. 6. DTG curves of PPC-based WPU films.

($T_{d,max}$) of different samples at the heating rate of 10 °C/min are shown in Table 3. It can be seen from Figs. 5 and 6, and Table 3 that the heat resistance of PPC-based WPU was significantly improved after modification with MCM-41 and MMT. $T_{d,0.05}$ of WPU was 189 °C, while for MCM-41/WPU, MMT/WPU and MCM-41-MMT(0.5)/WPU, they were 196, 198 and 212 °C, respectively. $T_{d,0.50}$ of PPC-based WPU films increased from 287 to 305, 310 and 312 °C by MCM-41 and MMT modification, respectively. From Table 3, it can be concluded that the single addition of MMT or MCM-41 could significantly improve the heat resistance of PPC-based WPU film, and due to the cooperative effect of MMT and

Table 3. Thermal degradation behavior of PPC-based WPU films

Samples	$T_{d,0.05}$ (°C)	$T_{d,0.10}$ (°C)	$T_{d,0.50}$ (°C)	$T_{d,max}$ (°C)
WPU	189	225	287	230
MCM-41/WPU	196	248	305	265
MMT/WPU	198	258	310	267
MCM-41-MMT(0.5)/WPU	212	261	312	266

$T_{d,0.05}$: temperature of 5% weight loss, $T_{d,0.10}$: temperature of 10% weight loss, $T_{d,0.50}$: temperature of 50% weight loss, $T_{d,max}$: temperature of maximum weight loss rate.

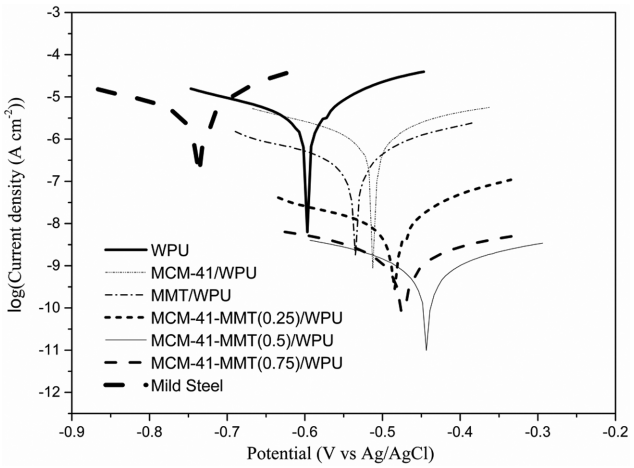

Fig. 7. Tafel curves of PPC-based WPU coatings.

MCM-41, MCM-41-MMT(0.5)/WPU film showed the best heat resistance. The results indicate that the cross-linking degree of PPC-based WPU film could be improved by adding MCM-41 or MMT alone, and the cross-linking degree of MCM-41-MMT(0.5)/WPU film was the highest due to the cooperative effect of MCM-41 and MMT.

2. Corrosion Performance Tests

2-1. Electrochemical Test

The corrosion resistance of PPC-based WPU coatings was studied by potentiodynamic polarization curve, and EIS and the Tafel curves of all PPC-based WPU coatings are shown in Fig. 7. For comparison, the polarization curve of bare mild steel is also shown in Fig. 7. For the polarization current test, the corrosion current (I_{corr}) and the corrosion potential (E_{corr}) are automatically gained from the Tafel curve by the CHI660D workstation analysis software [31]. The corrosion rate (R_c) was calculated by Eq. (2). [32]

$$R_c = \frac{k M_m I_{corr}}{n \rho_m} \quad (2)$$

Here k is the constant (3,268.5 mol A^{-1} a^{-1}), M_m is the molecular mass of iron (55.85 g mol^{-1}), the material density ρ_m=7.85 g cm^{-3} for mild steel, and the number of electrons was assumed to be 2. The percent protection efficiency values (E) were also obtained using Eq. (3) [33].

$$E\% = \frac{I_{corr} - I_{corr(C)}}{I_{corr}} \quad (3)$$

where I_{corr} and $I_{corr(C)}$ are the corrosion current values in absence and presence of the coatings, respectively. The corrosion current (I_{corr}), corrosion potential (E_{corr}), corrosion rate (R_c), and the percent protection efficiency values (E) are shown in Table 4.

In Fig. 7, both the anodic current and cathodic current of PPC-based WPU coatings decreased after adding MCM-41 or MMT, which illustrated that the addition of MMT and MCM-41 could effectively inhibit the cathode and anode reactions of the coatings. Compared with the addition of MMT or MCM-41 alone, the co-doping of layered MMT and mesoporous MCM-41 promoted the further decline of the corresponding I_{corr} values. Also, corrosion potential of MCM-41-MMT/WPU coatings was found to be higher than those of MCM-41/WPU or MMT/WPU samples. It indicates that the co-doping of of layered MMT and mesoporous MCM-41 could obtain better corrosion resistance than the addition of MMT or MCM-41 alone. For MCM-41-MMT/WPU coatings, with the increase of MMT and MCM-41, the corresponding I_{corr} values first decreased and then increased, and the corresponding corrosion potential showed a trend of first rising and then decreasing. MCM-41-MMT(0.5)/WPU showed the best corrosive resistance with a 1.12×10^{-11} A cm^{-2} of the corresponding I_{corr} value and a −0.444 V (Ag/AgCl) of the corresponding E_{corr} value.

As can be seen from Table 4, among all PPC-based WPU samples, MCM-41-MMT(0.5)/WPU showed the best protection efficiency of 99.99%. For comparison, the percent protection efficiency values (E) of diamine-based polybenzoxazine (Poly(Ph-mda)) anti-corrosion coating [34] and organoclays modified polybenzoxazine (PBI30-1) anti-corrosion coating [35] are also listed in Table 4. It can be seen from Table 4 that the percent protection efficiency value (E) of MCM-41-MMT(0.5)/WPU is better than those of Poly(Ph-mda) and PBI30-1 anti-corrosion coatings.

The above results show that the co-doping of layered MMT and mesoporous MCM-41 could effectively improve the barrier performance of PPC-based WPU coating. Layered MMT and mesoporous MCM-41 nanoparticles acted as a bridge to connect more molecules by occupying the pores formed by local shrinkage during the curing process of PPC-based WPU. It could lead to the

Table 4. Electrochemical parameters of the PPC-based WPU coatings in the elctrolyte

Samples	E_{corr}/V	I_{corr}/A·cm^{-2}	R_c/mm·a^{-1}	E/%
MS	−0.736	1.42×10^{-7}	1.65×10^{-3}	-
WPU	−0.596	6.31×10^{-9}	7.33×10^{-5}	95.55
MCM-41(1.0 wt.%)/WPU	−0.513	8.59×10^{-10}	9.98×10^{-6}	99.39
MMT(1.0 wt.%)/WPU	−0.535	1.72×10^{-9}	1.99×10^{-5}	98.78
MMT(0.25 wt.%)-MCM-41(0.25 wt.%)/WPU	−0.484	2.82×10^{-10}	3.28×10^{-6}	99.80
MMT(0.5 wt.%)-MCM-41(0.5 wt.%)/WPU	−0.444	1.12×10^{-11}	1.52×10^{-7}	99.99
MMT(0.75 wt.%)-MCM-41(0.75 wt.%)/WPU	−0.476	7.94×10^{-11}	9.23×10^{-7}	99.94
Poly(Ph-mda)-200 [34]	-	-	-	98.96
PBI30-3 [35]	-	-	-	93.26
PBI30-1 [35]	-	-	-	99.91

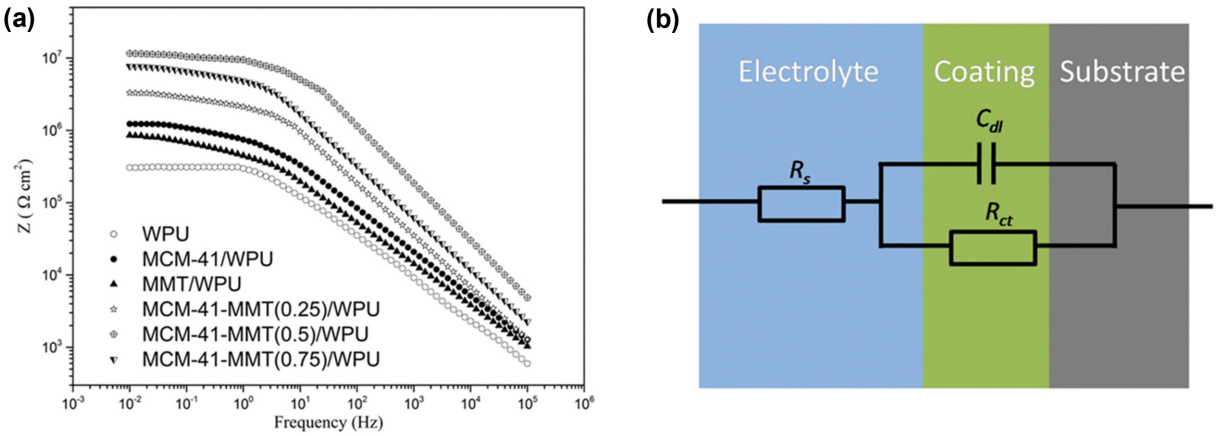

Fig. 8. (a) Bode plots of PPC-based WPU coatings measured in 3.5 wt% NaCl aqueous solution and (b) equovalent circuit model uesd in modeling.

Table 5. Parameters of the equivalent circuit in 3.5 wt% NaCl solutions

Samples	R_s (Ω cm^2)	R_{ct} (Ω cm^2)	C_{dl} (CPE)	
			Q (Ω^{-1} cm^2 s$^{\alpha}$)	α
WPU	82.5	3.05×10^5	4.18×10^{-5}	0.74
MCM-41/WPU	98.4	1.23×10^6	4.26×10^{-6}	0.63
MMT/WPU	78.6	8.54×10^5	1.64×10^{-5}	0.65
MCM-41-MMT(0.25)/WPU	121.8	3.31×10^6	2.34×10^{-7}	0.78
MCM-41-MMT(0.5)/WPU	115.4	1.16×10^7	5.22×10^{-8}	0.82
MCM-41-MMT(0.75)/WPU	118.3	7.69×10^6	1.21×10^{-7}	0.69

decrease of total free volume and the increase of compactness of PPC-based WPU coating. The nano network composite structure composed of completely exfoliated MMT, dispersed MCM-41 and PPC-based WPU was similar to the research conclusion of Wang et al. [25].

To better study the corrosion resistance of PPC-based WPU coatings, all samples were characterized by EIS and their electrochemical behavior was investigated. Fig. 8(a) presents bode plots for all the PPC-based WPU coatings measured in 3.5 wt% NaCl aqueous solution. In general, higher Z modulus at lower frequencies indicates better corrosion resistance of the coating on the substrate [36,37]. By fitting the experimental data with an appropriate equivalent circuit model, the corrosion resistance of different coatings can be analyzed in more detail [38]. All EIS data are fitted using a simple equivalent circuit model (as shown in Fig. 8(b)), which is usually used for coated mild steel [39]. The model includes the following elements: R_s (a resistor related to solution resistance), R_{ct} (the resistance of the coating-electrolyte interface inside the coating) and C_{dl} (the capacitance of the coating-electrolyte interface inside the coating). The constant phase element (CPE) is more suitable to describe the behavior of coatings with mesoporous structure and/or chemical heterogeneity [40]. Therefore, the ideal capacitance in the equivalent circuit is replaced by the constant phase element (CPE) to simulate the capacitance of the electric double layer on the metal/liquid interface. The CPE information is translated into an equivalent capacitance of C_{dl} and the specific information is Impedance $Z_{CPE}=1/Q\ (i\omega)^{\alpha}$ with i is an imaginary unit, ω is an angular frequency ($\omega=2\pi f$), α and Q is an exponential coefficient and a frequency-independent constant, respectively [40]. The calculated values of different coating parameters are shown in Table 5. The model is applied to fit the EIS data, and a good superposition with the experimental data is obtained. The parameters with uncertainty less than 3% in Table 5 demonstrated the reliability of the fitting results.

In the analysis of coating performance, R_s is not important either technically or theoretically because it is a property of the coating [41]. The addition of nanoparticles increasesd the charge transfer resistance R_{ct} and reduced the double-layer capacitance C_{dl}, indicating that the porosity of the coating was reduced and the corrosion resistance of the steel substrate was improved [42]. It can be seen from Table 5 that R_{ct} of WPU coating without MMT or MCM-41 was $3.05\times10^5\ \Omega$ cm^2, and those of MCM-41/WPU and MMT/WPU coatings were 1.23×10^6 and $8.54\times10^5\ \Omega$cm^2, which increased by 400% and 280%, respectively. Meanwhile, compared to WPU coating, C_{dl} was reduced by 90% and 61% for MCM-41/WPU and MMT/WPU coatings, respectively, indicating that the addition of MCM-41 and MMT could effectively improve the corrosive resistance of the PPC-based WPU coating.

For the MMT/WPU coating, as shown in the results of XRD (Fig. 2, curve (d)), the layer structure of MMT was intercalated, so the interaction between PPC-based WPU and the monolayer of MMT may lead to the improvement of the coating resistance. For MCM-41/WPU, XRD results also showed that there were PPC-based WPU chains existing in the mesoporous channels of MCM-

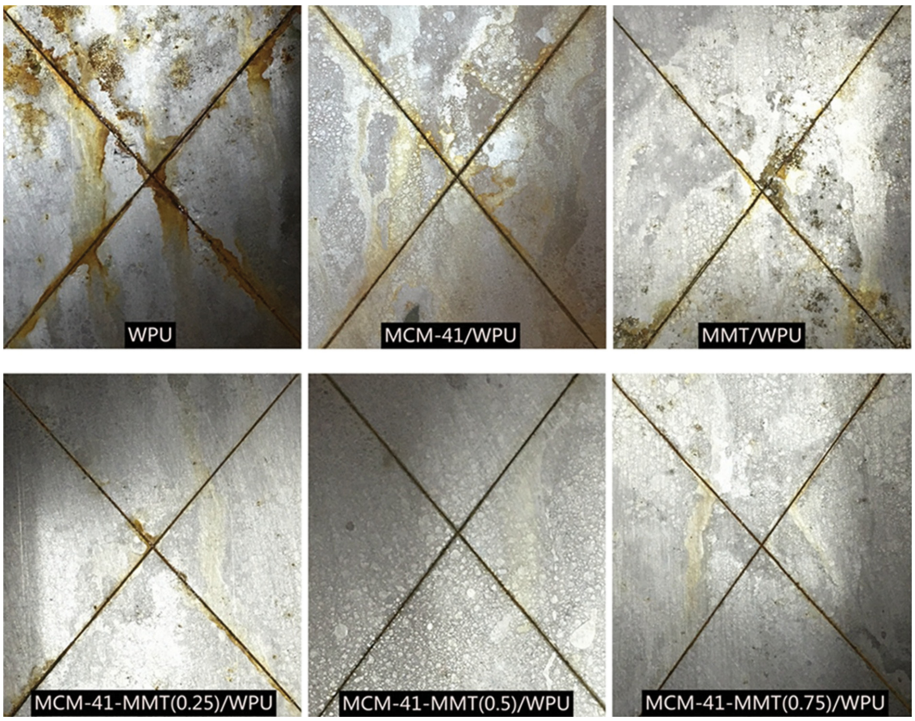

Fig. 9. Comparison of PPC-based WPU coatings after treatment in a humid chamber for 5 days.

41, which could effectively inhibit the accumulation of MCM-41 nanoparticles. In addition, the PPC-based WPU chain through the mesoporous channels of MCM-41 strengthened the interaction through the twist, twining and diffusion between the PPC-based WPU and the nannoparticles.

Compared with those of MCM-41/WPU and MMT/WPU coatings, R_{ct} of the MCM-41-MMT/WPU coatings showed a significant increase. For MCM-41-MMT/WPU coatings, with the increase of MMT and MCM-41, R_{ct} showed a trend of first increasing and then decreasing and MCM-41-MMT(0.5)/WPU showed the best corrosive resistance with a maximum value at $1.16\times10^7\ \Omega\ cm^2$, indicating the obvious effect of the addition amount of MCM-41 and MMT on the corrosive resistance of MCM-41-MMT/WPU coatings. Due to the synergistic effect of mesoporous MCM-41 and layered MMT, appropriate addition of MCM-41 and MMT could increase the compactness and shielding effect of the PPC-based WPU coating. However, the excessive addition of MCM-41 and MMT could lead to the increase of porosity and the decrease of compactness of the coating, and eventually lead to the decrease of the corrosive resistance of MCM-41-MMT/WPU. This was consistent with the result obtained from the Tafel curve.

The R_{ct} of the PPC-based WPU coating co-doping with MCM-41 and MMT was almost ten-times higher than that of WPU coating filled with nano MCM-41 or MMT alone. The results of XRD indicated that the MMT in the composite polyurethane resin was peeled off and WPU chains formed in the mesoporous channel of MCM-41 after grinding. Due to the mutual twist, twining and diffusion between the PPC-based WPU and the nannoparticles, the co-doping of MCM-41 and MMT ameliorated the interface interaction between the interfaces of the PPC-based WPU coatings. Due to the different shapes of mesoporous MCM-41 and layered MMT, the synergistic effect could lead to an enhancement of the cross-linking density and a decrease of the total free volume of the cured PPC-based WPU. For the MCM-41-MMT/WPU coating, the existence of PPC-based WPU chains in mesoporous channels promoted the good dispersion of MCM-41 particles in WPU matrix. MCM-41 acted as a bridge in the interconnect matrix and together with MMT made WPU form a more uniform coating during the curing process.

2-2. Salt Spray Tests

According to the electrochemical test results, MCM-41-MMT (0.5)/WPU coating provided the best corrosion protection for mild steel. To confirm this observation, the corrosive resistance of PPC-based WPU coatings was also evaluated by salt spray test, which was based on the corrosion and blistering of the coating surface on the mild steel substrate. The mild steel samples with PPC-based WPU coatings were scratched and exposed to a humid chamber over five days. Based on visual observations and the comparison in Fig. 9, the resistance against corrosion followed the following trend: MCM-41-MMT(0.5)/WPU>MCM-41-MMT(0.25)/WPU~MCM-41-MMT(0.75)/WPU>MCM-41/WPU>MMT/WPU>WPU. The results of salt spray tests were consistent with those of Tafel curves and EIS, indicating that the co-doping of mesoporous MCM-41 and layered MMT could effectively prevent the PPC-based WPU coatings from blistering and rusting.

CONCLUSIONS

PPC-based WPU was prepared with PPC as the soft segment, IPDI and BDO as the hard segments, DMBA as the donors of

hydrophilic groups and TMP as the cross-linking agent. The effect of co-doping of layered MMT and mesoporous material MCM-41 on the corrosion resistance of PPC-based WPU resin was investigated. The results of Tafel curves, EIS and salt spray tests showed that the co-doping of mesoporous MCM-41 and layered MMT could improve the barrier performance of PPC-based WPU without MMT and MCM-41, make water and ions hard to migrate, and reduce the tendency of substrate rusting and coating blistering. MCM-41-MMT(0.5)/WPU coating represented the best corrosive resistance in all the samples. The mechanism of the enhancement of corrosive resistance of MMT-MCM-41/WPU coating could be attributed to the cross-linking of exfoliated layered MMT and MCM-41 with PPC-based WPU chain in the mesoporous channel. The cross-linking structure of MMT and MCM-41 particles was helpful to form the compact nanocomposite coating, thus improving the corrosive resistance of the coating.

ACKNOWLEDGEMENT

The authors gratefully acknowledge the financial support from Science and Technology Project of Hebei Education Department (Grant No.:Z2019033).

DECLARATION OF CONFLICTING INTERESTS

The author(s) declared no potential conflicts of interest with respect to the research, authorship, and/or publication of this article.

REFERENCES

1. S. S. Pathak, A. Sharma and A. S. Khanna, *Prog. Org. Coat.*, **65**, 206 (2009).
2. A. Noreen, K. M. Zia, M. Zuber, S. Tabasum and M. J. Saif, *Korean J. Chem. Eng.*, **2**, 388 (2016).
3. B. Özbek and Ş. Ünal, *Korean J. Chem. Eng.*, **7**, 1992 (2017).
4. T. A. Phan, F. X. Perrin and L. Nguyen-Dinh, *Korean J. Chem. Eng.*, **35**, 1365 (2018).
5. D. Snihirova, S. V. Lamaka and M. F. Montemor, *Electrochim. Acta*, **83**, 439 (2012).
6. H. Li, J. Wang, J. Yang, J. Zhang and H. Ding, *Prog. Org. Coat.*, **143**, 105607 (2020).
7. S. Pathan and S. Ahmad, *Prog. Org. Coat.*, **122**, 189 (2018).
8. O. Rahman, M. Kashif and S. Ahmad, *Prog. Org. Coat.*, **80**, 77 (2015).
9. J. Ding, O. Rahman, W. Peng, H. Dou and H. Yu, *Appl. Sur. Sci.*, **427**, 981 (2018).
10. S. K. Dhoke, T. J. M. Sinha, P. Dutta and A. S. Khanna, *Prog. Org. Coat.*, **62**, 183 (2008).
11. J. Li, J. Cui, J. Yang, Y. Li, H. Qiu and J. Yang, *Compos. Sci. Technol.*, **129**, 30 (2016).
12. Z. Li, Y. Qin, X. Zhao, F. Wang, S. Zhang and X. Wang, *Eur. Polym. J.*, **47**, 2152 (2011).
13. F. Gao, Q. Zhou, Y. Dong, Y. Qin, X. Wang, X. Zhao and F. Wang, *J. Polym. Res.*, **19**, 9877 (2012).
14. X. Zhang, F. Wang and Y. Du, *Surf. Coat. Tech.*, **201**, 7241 (2007).
15. Y. Shao, C. Jia, G. Meng, T. Zhang and F. Wang, *Corros. Sci.*, **51**, 371 (2009).
16. H. Shi, F. Liu, L. Yang and E. Han, *Prog. Org. Coat.*, **62**, 359 (2008).
17. M. Behzadnasab, S. M. Mirabedini, K. Kabiri and S. Jamali, *Corros. Sci.*, **53**, 89 (2011).
18. X. Shi, T. A. Nguyen, Z. Suo and Y. Liu, *Surf. Coat. Tech.*, **204**, 237 (2009).
19. W. Ji, J. Hu, L. Liu, J. Zhang and C. Cao, *Surf. Coat. Tech.*, **201**, 4789 (2007).
20. A. Wolińska-Grabczyk, M. Wojtowicz, A. Jankowski, E. Grabiec, P. Kubica, M. Musioł and M. Sobota, *Polymer*, **158**, 32 (2018).
21. Z. Li, A. J. González, V. B. Heeralal and D. Wang, *Compos. Part B-Eng.*, **138**, 101 (2018).
22. R. L. Lavall, S. Ferrari, C. Tomasi, M. Marzantowicz, E. Quartarone, M. Fagnoni, P. Mustarelli and M. L. Saladino, *Electrochim. Acta*, **60**, 359 (2012).
23. N. Wang, C. Zhao, Z. Shi, Y. Shao, H. Li and N. Gao, *Mater. Sci. Eng. B-Adv.*, **157**, 44 (2009).
24. N. Wang, Y. Shao, Z. Shi, J. Zhang and H. Li, *J. Mater. Sci.*, **43**, 3683 (2008).
25. N. Wang, K. Cheng, H. Wu, C. Wang, Q. Wang and F. Wang, *Prog. Org. Coat.*, **75**, 386 (2012).
26. J. Yeh, H. Huang, C. Chen, W. Su and Y. Yu, *Surf. Coat. Tech.*, **200**, 2753 (2006).
27. S. Chen, Z. Hua, Z. Fang and G. Qi, *Polymer*, **45**, 6519 (2004).
28. M. A. Alam, U. A. Samad, R. Khan, M. Alam and S. M. Al-Zahrani, *Korean J. Chem. Eng.*, **8**, 2301 (2017).
29. M. M. Rahman, R. Suleiman and H. D. Kim, *Korean J. Chem. Eng.*, **9**, 2480 (2017).
30. X. Li, Y. Meng, Q. Zhu and S. C. Tjong, Polym. *Degrad. Stabil.*, **81**, 157 (2003).
31. P. Wang, D. Zhang and Z. Lu, *Corros. Sci.*, **90**, 23 (2015).
32. W. Sun, L. D. Wang, T. T. Wu, Y. Q. Pan and G. C. Liu, *Carbon*, **79**, 605 (2014).
33. C. L. Zhou, X. Lu, Z. Xin, J. Liu and Y. F. Zhang, *Prog. Org. Coat.*, **76**, 1178 (2013).
34. X. Y. Zhang, X. Lu, R. Zhang, C. L. Zhou and Z. Xin, *J. East China Univ. Techno.: Nat. Sci. Ed. (in Chinese)*, **43**, 614 (2017).
35. C. L. Zhou, X. Lu, Z. Xin and Y. F. Zhang, *J. Coat. Technol. Res.*, **13**, 63 (2016).
36. D. Zhu and W. J. Ooij, *Corros. Sci.*, **45**, 2177 (2003).
37. R. Naderi and M. M. Attar, *Corros. Sci.*, **52**, 1291 (2010).
38. E. D. Mekeridis, I. A. Kartsonakis and G. C. Kordas, *Prog. Org. Coat.*, **73**, 142 (2012).
39. M. Behzadnasab, S. M. Mirabedini, K. Kabiri and S. Jamali, *Corros. Sci.*, **53**, 89 (2011).
40. D. Prasai, J. C. Tuberquia, R. R. Harl, G. K. Jennings and K. I. Bolotin, *ACS Nano*, **6**, 1102 (2012).
41. X. Shi, T. A. Nguyen, Z. Suo, Y. Liu and R. Avci, *Surf. Coat. Technol.*, **204**, 237 (2009).
42. H. Yun, J. Li, H. B. Chen and C. J. Lin, *Electrochim. Acta*, **52**, 6679 (2007).